Adult spinal motoneurons change their neurotransmitter phenotype to control locomotion

Maria Bertuzzi[a,1], Weipang Chang[a,1], and Konstantinos Ampatzis[a,2]

[a]Department of Neuroscience, Karolinska Institutet, 171 77 Stockholm, Sweden

Edited by Nicolas C. Spitzer, University of California, San Diego, La Jolla, CA, and approved September 11, 2018 (received for review May 25, 2018)

A particularly essential determinant of a neuron's functionality is its neurotransmitter phenotype. While the prevailing view is that neurotransmitter phenotypes are fixed and determined early during development, a growing body of evidence suggests that neurons retain the ability to switch between different neurotransmitters. However, such changes are considered unlikely in motoneurons due to their crucial functional role in animals' behavior. Here we describe the expression and dynamics of glutamatergic neurotransmission in the adult zebrafish spinal motoneuron circuit assembly. We demonstrate that part of the fast motoneurons retain the ability to switch their neurotransmitter phenotype under physiological (exercise/training) and pathophysiological (spinal cord injury) conditions to corelease glutamate in the neuromuscular junctions to enhance animals' motor output. Our findings suggest that motoneuron neurotransmitter switching is an important plasticity-bestowing mechanism in the reconfiguration of spinal circuits that control movements.

neuromuscular junction | motoneurons | zebrafish | exercise | injury

Neuronal communication involves the release and uptake of specific neurotransmitters (1, 2)—endogenous chemical messengers that participate in diverse biological processes by conveying intercellular signals across synapses. All spinal interneurons and motoneurons derive from fixed locations in the spinal cord and express stereotypic combinations of transcription factors during their early development (3–8) that determine their identity and assign them the expression of a specific transmitter phenotype. Therefore, the adoption of a neurotransmitter by a neuron defines its anatomical and functional identity.

Motoneurons, the output neurons of the nervous system, are responsible for the execution of all animals' movements. Vertebrate motoneurons were traditionally thought to mediate their actions on both muscles and Renshaw cells exclusively through cholinergic transmission (9–11). Recent evidence indicates that they also release glutamate as a neurotransmitter during early development to mediate exclusively central functions (12–15). However, the ability of well-developed adult motoneurons to express and release glutamate still remains unclear.

A major unresolved issue in neuroscience is how neurons react to changes. The prevailing view is that neurotransmitter phenotypes are fixed and determined early during development. However, an emerging consensus from recent studies is that their phenotypes are plastic and mediated by the gain or loss of an additional neurotransmitter (16–18). This provides a putative homeostatic mechanism for harmonizing the activity of the well-orchestrated neuronal circuits (19). While it is not yet clear which neurons specifically undergo neurotransmitter changes, it has been assumed that the neurotransmission phenotype of essential neurons for the circuits, such as the motoneurons, lacks such plasticity (19, 20).

Using a combination of anatomical, electrophysiological, pharmacological, and in vivo behavioral approaches in the adult zebrafish, we reveal a previously unsuspected dynamic coexpression of glutamate in adult spinal motoneuron circuit assembly. We demonstrate that physical activity and spinal cord injury (SCI) can respecify the neurotransmitter phenotype of the fast motoneurons. This dynamic coexpression and corelease of Ach and glutamate in the adult vertebrate neuromuscular junctions (NMJs) aims to regulate and fine-tune motor behaviors in vertebrates.

Results

Axial Motoneurons Express Glutamate. We sought to determine whether adult zebrafish spinal motoneurons are also glutamatergic by combining retrograde labeling of motoneurons with glutamate immunostaining (Fig. 1*A*). We observed that 21.41 ± 1.091% (n = 12 zebrafish) of the labeled motoneurons were expressing glutamate (Fig. 1*B*) distributed in an area similar to that of the nonglutamate-expressing motoneurons (Fig. 1*C*). To determine the presence of these dual phenotype neurons in different motoneuron pools, we exploited the accessible neuromuscular configuration of adult zebrafish (21) by performing focal injections of a dextran retrograde tracer into slow, intermediate, and fast muscle fibers (21). We found that 42.67 ± 2.245% of slow (n = 12 zebrafish), 26.32 ± 1.911% of intermediate (n = 13 zebrafish), and 18.07 ± 1.036% of fast (n = 16 zebrafish) secondary motoneurons, but not the primary motoneurons (n = 12 zebrafish), were expressing glutamate (Fig. 1 *D* and *E*). Moreover, analysis of the soma sizes and locations of the motoneurons indicated that glutamate was expressed by higher proportions of fast motoneurons with relatively small somas and more ventral positions (Fig. 1*F*). Together, these results confirmed that part of the spinal motoneurons in adult zebrafish exhibit a dual neurotransmitter phenotype.

Significance

An intriguing feature of the nervous system is its plasticity—the remarkable lifelong capacity to change and adapt in light of intrinsic and extrinsic stimuli. Among the many different adaptive mechanisms that occur within the nervous system, changes in neurotransmission form an important plasticity-bestowing mechanism in the reconfiguration of neuronal circuits. Here, we reveal that physical activity and spinal cord injury can switch the neurotransmitter phenotype of the fast axial motoneurons to coexpress glutamate. Furthermore, our study shows that the adult vertebrate spinal motoneurons corelease glutamate alongside ACh in neuromuscular junctions to regulate motor behaviors. Thus, our findings suggest that fast motoneuron glutamatergic respecification enables a motor function-enhancing mechanism in vertebrates.

Author contributions: K.A. designed research; M.B., W.C., and K.A. performed research; M.B., W.C., and K.A. analyzed data; and M.B., W.C., and K.A. wrote the paper.

The authors declare no conflict of interest.

This article is a PNAS Direct Submission.

[1]M.B. and W.C. contributed equally to this work.

[2]To whom correspondence should be addressed. Email: konstantinos.ampatzis@ki.se.

This article contains supporting information online at www.pnas.org/lookup/suppl/doi:10.1073/pnas.1809050115/-/DCSupplemental.

Published online October 1, 2018.

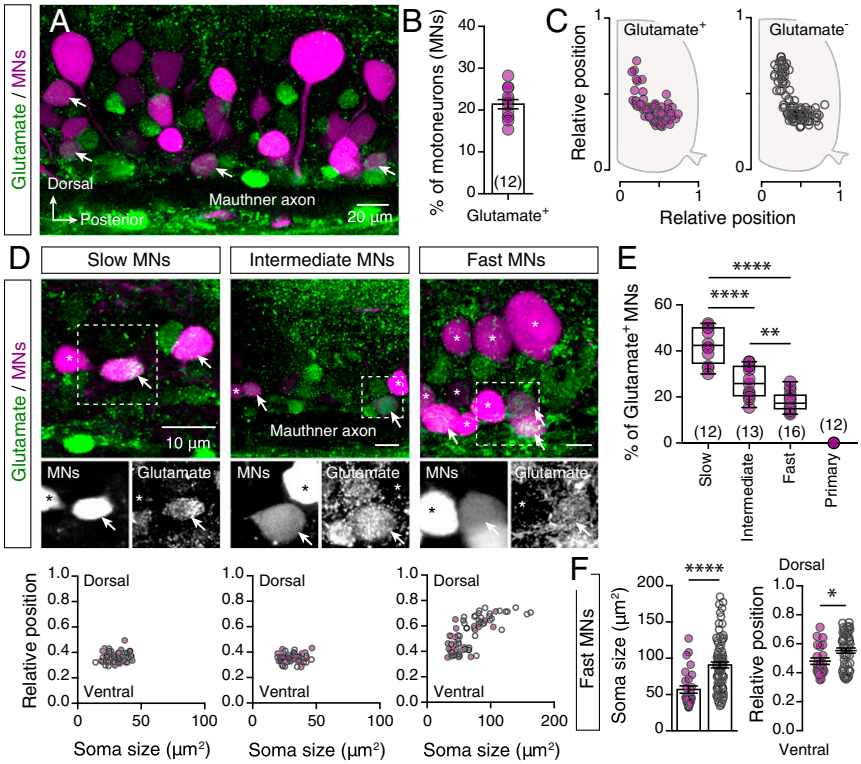

Fig. 1. Analysis of the glutamatergic phenotype of adult spinal motoneurons. (*A*) Whole-mount fluorescence image of retrogradely traced motoneurons (MNs; magenta) and glutamate immunohistochemistry (green). (*B*) Percentages of the retrogradely traced motoneurons that express glutamate (n = 12 zebrafish). (*C*) Spatial distributions of the glutamate$^+$ (solid circles) and glutamate$^-$ (open circles) immunoreactive motoneurons (n = 5 zebrafish). (*D*) Whole-mount immunofluorescent images (*Top*) showing the glutamatergic expression (green) in different motoneuron pools (magenta). Analysis of the soma sizes and dorsoventral locations of the glutamate and nonglutamate expressing motoneurons (*Bottom*). (*E*) The significantly differing percentages of retrogradely traced motoneurons that express glutamate in slow, intermediate, and fast pools ($P < 0.0001$, one-way ANOVA). (*F*) Glutamate-positive fast motoneurons (solid circles) were smaller ($P < 0.0001$, unpaired t-test) and located more ventrally ($P = 0.0208$, unpaired t-test) than the nonglutamate fast motoneurons (open circles). Arrows indicate the double-labeled cells. Asterisks indicate glutamate immunonegative motoneurons. Data are presented as mean ± SEM and as box plots showing the median and 25th and 75th percentile (box and line) and minimal and maximal values (whiskers). *$P < 0.05$; **$P < 0.01$; ****$P < 0.0001$. For detailed statistics see *SI Appendix*, Table S1.

Dynamic Expression of the Motoneuron Glutamatergic Phenotype. Is motoneuron neurotransmission plastic? To evaluate the ability of motoneurons to change their neurotransmitter phenotype, we subjected a set of animals to forced swim training and another set to SCI (*Materials and Methods* and *SI Appendix*, Fig. S1) to induce adaptive responses in the spinal cord to physiological and pathophysiological stimuli, respectively. While neither treatment changed the number (Fig. 2*B*) or cholinergic phenotype (*SI Appendix*, Fig. S2) of axial motoneurons, both perturbations significantly increased the proportion of glutamate-labeled motoneurons, from 21.41 ± 1.091% (n = 12 zebrafish) to 39.54 ± 3.014% (n = 7 zebrafish) in trained animals and 33.21 ± 1.884% (n = 7 zebrafish) in animals subjected to spinal cord lesion [one-way ANOVA: $F_{(2,23)} = 26.55$, $P < 0.0001$; Fig. 2 *A* and *C*]. More specifically, the proportion of glutamatergic cells in the slow and intermediate motoneuron pools was unchanged (Fig. 2*D*), but there were clear changes in the fast motoneuron pool [one-way ANOVA: $F_{(4,33)} = 17.65$, $P < 0.0001$; Fig. 2*E*]: The percentage of glutamate-positive fast motoneurons (17 ± 0.952%, n = 12 zebrafish) increased significantly after training (38.29 ± 3.735%, n = 7 zebrafish) or spinal cord lesion (33.08 ± 1.918%, n = 9 zebrafish; Fig. 2*E*). Analysis of the glutamate-positive motoneurons' soma sizes and positions revealed that the larger fast motoneurons [one-way ANOVA: $F_{(2,174)} = 4.738$, $P = 0.0099$; Fig. 2*E*] located in the more dorsal part of the motor column [one-way ANOVA: $F_{(2,117)} = 4.917$, $P = 0.0089$; Fig. 2*E*] switched to a glutamatergic phenotype. Finally, 4 wk of rest from training or recovery from SCI restored the percentage of glutamatergic neurons to that in control animals (Fig. 2*E*), suggesting that the fast motoneuron glutamatergic phenotype respecification is dynamic and reversible (Fig. 2*F*).

Although both of the preconditioning stimuli directly target the animal's locomotion machinery, their observed effects do not exclude the possibility that dynamic expression of the glutamatergic phenotype in motoneurons may be triggered by other nonmotor-related stimuli that affect the spinal cord indirectly. To test this possibility, we also subjected adult zebrafish to a previously reported sterile inflammation treatment (22) involving i.p. injection with antigenic LPS particles that mimic a gram-negative bacterial infection or zymosan (which simulates a fungal infection) to induce an acute sterile inflammatory response (*Materials and Methods* and *SI Appendix*, Fig. S3). Following both perturbations, the proportion of glutamatergic motoneurons remained unchanged a week after the onset of inflammation (*SI Appendix*, Fig. S3), suggesting that the previously observed switch in motoneuron glutamatergic phenotype is directly associated with the animal's motility.

Together our results demonstrate that there are three distinct pools of axial motoneurons: two "core pools" expressing either ACh alone or both ACh and glutamate and a primarily cholinergic "reserve pool" that may also become glutamatergic in a reversible manner (Fig. 2*F*). Motoneurons of the reserve pool are fast secondary motoneurons, which are responsible for generation of fast swimming and escape responses (21). Thus, our

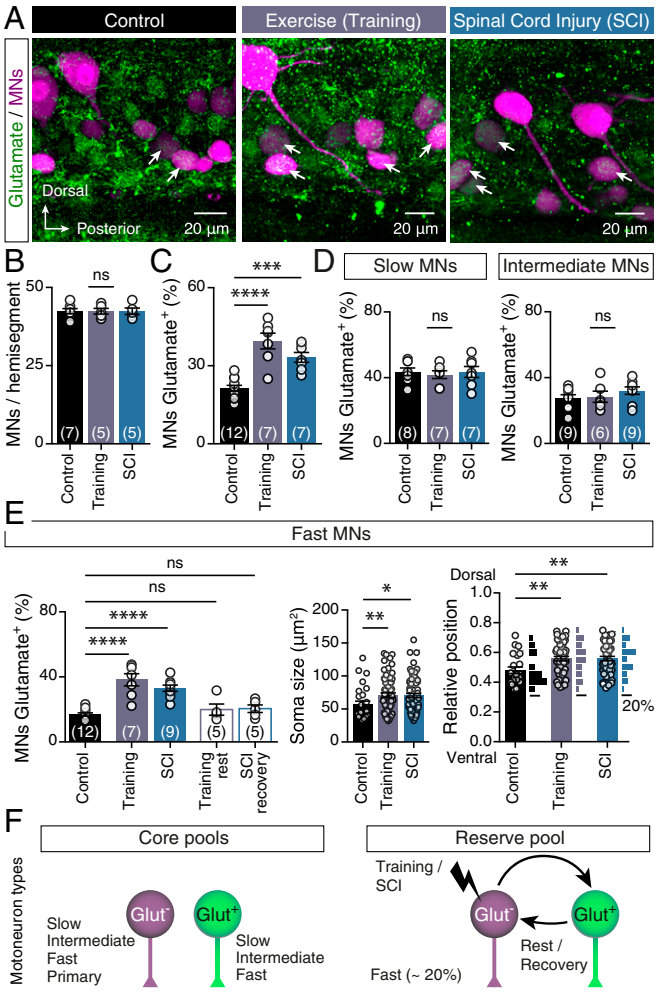

Fig. 2. Respecification of motoneuron glutamatergic phenotype. (*A*) Representative whole-mount confocal images showing glutamatergic expression in axial motoneurons (MNs) of control animals, after swim training and after SCI. (*B*) Quantification of numbers of axial motoneurons. (*C*) Changes in percentages of axial motoneurons that coexpressed glutamate after swim training or SCI ($P < 0.0001$, one-way ANOVA). (*D*) The percentage of slow and intermediate motoneurons that expressed glutamate remained unchanged following these perturbations. (*E*) The percentage of glutamate$^+$ fast motoneurons increased after training or SCI ($P < 0.0001$, one-way ANOVA). Quantification of soma sizes and locations of the glutamate$^+$ fast motoneurons suggests that the larger motoneurons ($P = 0.0099$, one-way ANOVA) located in the dorsal part ($P = 0.0089$, one-way ANOVA) of the motor column retain ability to respecify their neurotransmitter phenotype. (*F*) Schematic representation of the three distinct pools of motoneurons observed in adult zebrafish spinal cord. Approximately 20% of the fast motoneurons constitute the reserve pool and retain ability to respecify their neurotransmitter phenotype. Arrows indicate the double-labeled cells. Data are presented as mean ± SEM; *$P < 0.05$; **$P < 0.01$; ***$P < 0.001$; ****$P < 0.0001$; ns, not significant. For detailed statistics see *SI Appendix*, Table S1.

findings imply that switches in motoneurons' neurotransmitter phenotypes in response to changes in environmental demands may participate in regulation of motor outputs.

Functional Significance of Motoneuron Glutamatergic Respecification. To probe possible associations between fast motoneuron glutamatergic respecification and changes in swimming behavior, animals were subjected to an open field test (Fig. 3*A*). Gross behavioral analyses revealed pronounced changes in the locomotor speed of trained animals (Fig. 3*B*), which, unlike controls, performed spontaneous high-velocity swim bouts (unpaired *t* test: $t = 4.361$, df = 10, $P = 0.0014$; Fig. 3*C*). Moreover, critical speed tests (*Materials and Methods*) showed that trained animals could swim faster than controls (unpaired *t* test: $t = 4.847$, df = 17, $P = 0.0002$; Fig. 3*D*). This outcome was unexpected since adult zebrafish rely solely on activation of their slow and intermediate neuromuscular systems for swimming at below ∼70% of their critical speed (U_{CRIT}; maximum speed of locomotion) (23). Indeed, exercise-induced contractile activity at below 70% of U_{CRIT} (as enforced in our training paradigm) resulted in selective adaptive responses (hypertrophy and hyperplasticity; Fig. 4) in slow and intermediate muscle fibers, and thus presumably in the slow and intermediate neurocircuitry, but not in the fast neurocircuitry that determines the maximum speed of locomotion. This suggests that muscle fiber remodeling was not responsible for the observed increases in trained animals' swimming speeds, and that fast motoneuron glutamatergic respecification may shift the operational range of the locomotor system.

To test the possibility that fast motoneuron glutamatergic respecification was responsible for the animals' ability to swim faster following our perturbations, we next investigated where the motoneurons released glutamate. Earlier studies have shown that glutamatergic responses of mammalian spinal motoneurons excite Renshaw cells and other motoneurons, but not muscles (13–15). However, in zebrafish, motoneurons do not have profound axonal collaterals capable of mediating central responses (21), no Renshaw cells have been detected in the spinal cord, and motoneuron–motoneuron communication relies on dendrodendritic electrical gap junctions (24). Therefore, we postulated that the motoneurons might release glutamate into the muscles together with ACh to enhance muscle contraction. To test this hypothesis, we first examined the presence of glutamate in the different muscle fibers (Fig. 5*A*). We found that glutamate immunolabeling intensities were highest, intermediate, and the lowest in the slow, intermediate, and fast muscle fibers, respectively [repeated measures (RM) one-way ANOVA: $F_{(1.216,6.079)} = 39.07$, $P = 0.0006$; Fig. 5*B*], similar to our previous observations of the proportions of glutamate-expressing motoneuron types (Fig. 1*E*). Consistent with motoneuron glutamatergic respecification pattern, we also observed that the intensity of glutamate expression was only significantly increased in the fast muscle fibers after training and SCI [one-way ANOVA (fast): $F_{(2,18)} = 8.775$, $P = 0.0022$; Fig. 5*C*]. We detected no significant differences in the number of NMJs under either applied perturbation (*SI Appendix*, Fig. S4), suggesting strong correspondence between increases in glutamate levels in fast muscles and fast motoneuron glutamatergic respecification.

To evaluate further whether axial motoneurons may account for the glutamate observed in the muscles, we examined the distribution of vesicular glutamate transporters (VGluTs), which are present in all neurons that release glutamate as a transmitter (25). We detected expression of VGluT1, but not VGluT2, in the area surrounding the muscle fibers (Fig. 5*D*). We also observed close apposition of VGluT1 in the NMJs (Fig. 5*D*) and numerous colocalizations and close proximities with VAChT (a specific transporter of cholinergic neurons) (26), indicating that the adult motoneurons host cellular machinery that enables them to release glutamate along with ACh.

Next, we tested the functional effects of glutamate on adult NMJs, by acquiring endplate current (EPC) recordings from isolated adult muscles (Fig. 5*E*). Application of the glutamate receptor agonist NMDA increased the EPC frequency in muscle fibers [one-way ANOVA (slow): $F_{(2,18)} = 11$, $P = 0.0008$; one-way ANOVA (fast): $F_{(2,21)} = 10.82$, $P = 0.0006$; Fig. 5*E*]. This increase was prevented by the selective NMDA receptor antagonist AP-5 (50 µM; Wilcoxon test: $P = 0.3125$, $n = 5$ zebrafish; *SI Appendix*, Fig. S5*A*). In addition, the nicotinic ACh receptor antagonists *d*-tubocurarine and α-bungarotoxin (α-BTX) and the selective blocker of choline uptake hemicholinium-3, which interferes with ACh synthesis, abolished all EPC signals, and this

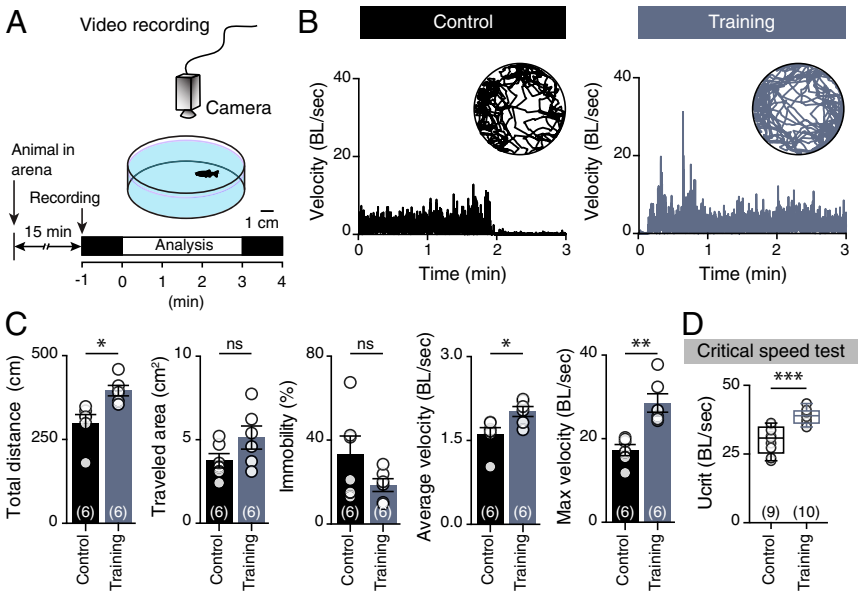

Fig. 3. Trained animals can swim faster. (*A*) Experimental design to investigate locomotor behavior of control and trained animals in an open field test. (*B*) Representative traces of the recorded animals' movements during the open field test and analysis of their normalized velocity (BL per s). (*C*) Quantification of the motor behavior parameters: maximum velocity ($P = 0.0014$, unpaired *t*-test), average velocity ($P = 0.022$, unpaired *t*-test), and total distance traveled ($P = 0.0106$, unpaired *t*-test). (*D*) Trained animals can swim faster than the control animals during critical speed tests ($P = 0.0002$, unpaired *t*-test). Speed is normalized (BL per s). Data are presented as mean ± SEM (*C*) and boxplots showing the median and 25th and 75th percentile (box and line) and minimal and maximal values (whiskers in *D*). $*P < 0.05$; $**P < 0.01$; $***P < 0.001$; ns, not significant. For detailed statistics see *SI Appendix*, Table S1.

effect was not reversed by further application of NMDA (*SI Appendix*, Fig. S5 *B–D*). These findings imply that the glutamate NMDA receptors are located in presynaptic motoneuron terminals. In addition, the presence of the noncompletive antagonist of the NMDA receptors (MK-801, 1 mM) in the intracellular solution induces no change in frequency of the recorded EPCs (*SI Appendix*, Fig. S5*E*), suggesting the absence of postsynaptic NMDA receptors in the NMJs. To further evaluate if motoneurons can also actively release glutamate, we electrically stimulated the spinal cord to depolarize the motoneurons while recording EPCs from muscle fibers (Fig. 5*F* and *SI Appendix*, Fig. S6). We observed significant reductions in EPC events following stimulation by blocking the NMDA receptors (AP-5; Fig. 5*F*). We also obtained anatomical support for the electrophysiological data, as the motoneuron axons innervating the musculature were decorated with NMDA-2A receptor subunits (*SI Appendix*, Fig. S5 *F* and *G*), while NMDA-2B receptors were observed specifically in the presynaptic terminals of NMJs (Fig. 5*G*). Together our findings indicate that adult zebrafish motoneurons can release both ACh and glutamate, but only ACh acts on postsynaptic muscles (through nicotinic AChRs), while glutamate acts on presynaptic NMDA receptors and facilitates ACh release (Fig. 5*H*), which is similar to previous reports for the developing vertebrate motoneurons (27–29). Finally, consistently with our previous results, we observed a significant increase in EPC event frequency in the fast muscles after training or SCI [one-way $ANOVA_{(Saline)}$: $F_{(2,30)} = 4.531$, $P = 0.0191$; Fig. 5*I*; one-way $ANOVA_{(NMDA)}$: $F_{(2,25)} = 5.549$, $P = 0.01$; *SI Appendix*, Fig. S7], suggesting that fast motoneuron glutamatergic respecification could potentially account for the increased release of glutamate in the fast NMJs.

Discussion

Our work demonstrates the glutamatergic identity of adult zebrafish spinal motoneurons and its plasticity. Since the first demonstration of vertebrate neuromuscular communication (9), NMJs have generally been considered relatively simple cholinergic synapses (9). Previous studies have raised the possibility that other neurotransmitters, such as glutamate (30–33), may also act on vertebrate NMJs, but their physiological actions have remained unclear. Here we demonstrate that spinal motoneurons innervating the axial musculature in adult zebrafish can coexpress and corelease glutamate into the NMJs to enhance the motor output. Our findings are consistent with previous indications that during the early development of both *Xenopus* tadpoles (27, 28) and zebrafish larvae (29) the spinal motoneurons can corelease glutamate and ACh in the NMJs. However, the possible presence of this mechanism in mammalian systems is still controversial. Earlier studies have indicated that mammalian spinal motoneurons can only release glutamate to mediate exclusively central functions (13–15), although motoneurons that innervate esophagus muscles in adult mice can reportedly release both glutamate and ACh into their NMJs (34). Clearly, further investigations are needed to elucidate variations in the nature of neuromuscular communication in different taxa, developmental stages, and organs to understand the evolutionary diversity and convergence of these synapses.

Inter alia, it is well-established that motoneurons are cholinergic but can also express and release glutamate during their development (12–15, 27–29, 32), but the dynamic nature of this phenomenon in adulthood has not been previously examined. Here, we reveal a previously unsuspected role of adult motoneuron transmitter phenotype respecification in responses to (patho)physiological changes. Historically, the neurotransmitter phenotype of a mature neuron has been considered fixed. However, recent studies on various vertebrates and areas of the nervous system clearly demonstrate that neurons' transmission programs can be reconfigured promptly and reversibly (17, 19, 20, 35–37). As transmitter respecification occurs in neurons that are already integrated into active and established neuronal networks, it does not affect their neuronal identity. Therefore, these neurons form so-called reserve pools (17, 19, 36, 37) that provide an embedded plasticity mechanism, which bestows neuronal circuits with flexibility and adaptability to changing environmental demands. Our findings reveal the existence of a reserve

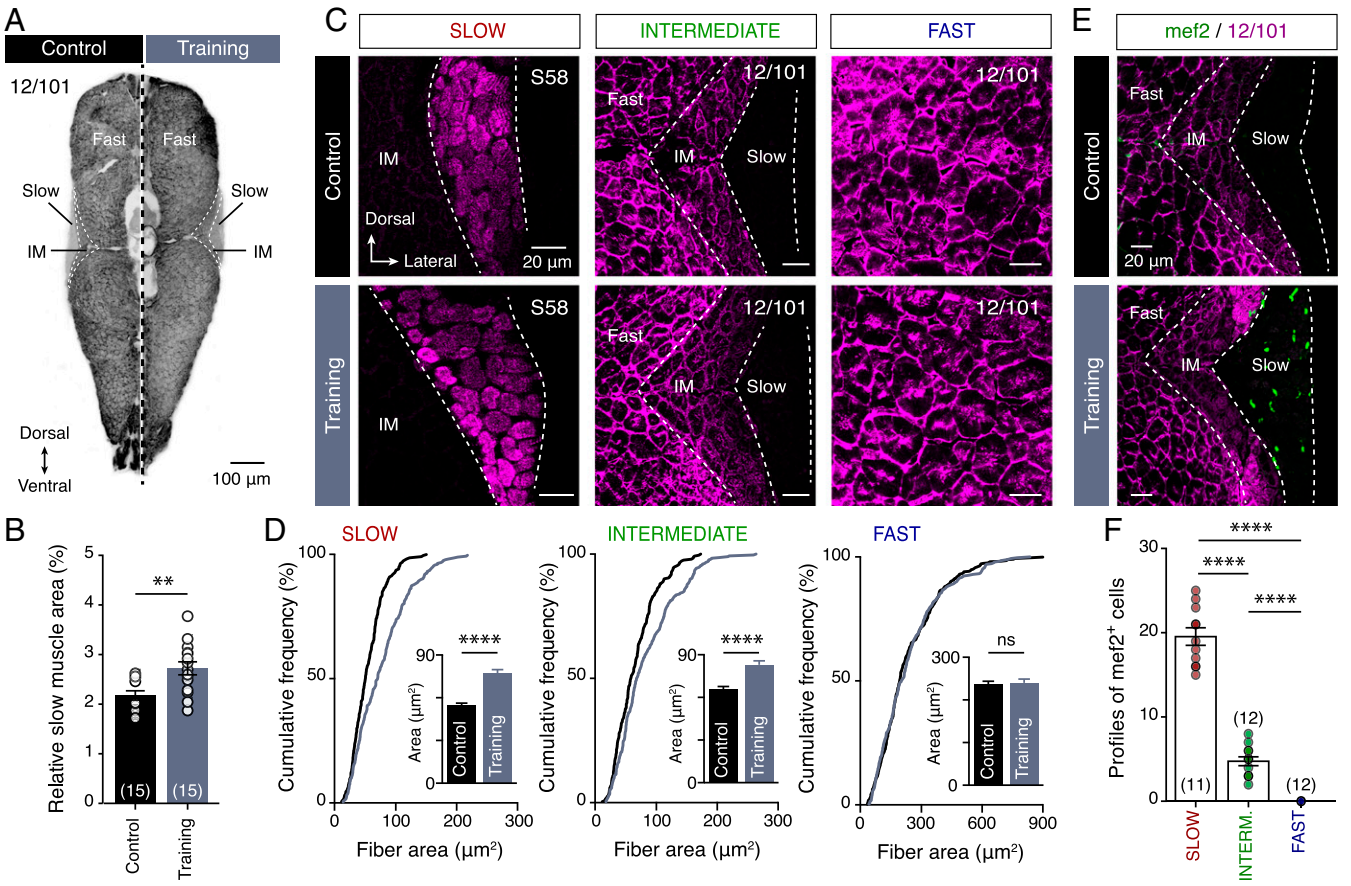

Fig. 4. Swim training induces selective muscle fiber hyperplastic and hypertrophic remodeling. (*A*) Whole-myotome microphotograph showing apparent increase in the area occupied by slow muscle fibers. (*B*) Quantification of the relative area within the myotome occupied by slow muscle fibers, showing it was significantly larger in trained animals than in controls ($P = 0.0022$, unpaired t test). (*C*) Representative confocal images showing the muscle fibers (slow, intermediate, and fast) of control and trained animals. (*D*) Quantification of the muscle fibers perimeters, showing that were significantly larger (indicating hypertrophy) in the slow ($P < 0.0001$, unpaired t test) and intermediate ($P < 0.0001$, unpaired t test) muscles of the trained animals compared with the controls. (*E* and *F*) Confocal photomicrographs and quantification demonstrating the absence of early differentiated myocytes (mef2$^+$, indicating hyperplasticity) in the control animals and fast muscle fibers of the trained animals ($P < 0.0001$, one-way ANOVA). Data are presented as mean ± SEM; $^{**}P < 0.01$; $^{****}P < 0.0001$; ns, not significant. For detailed statistics see *SI Appendix*, Table S1.

pool of fast motoneurons that are initially cholinergic but can also express glutamate in response to activity-dependent or pathological changes. This response also coincides with the enhancement of the locomotor system's operational range.

Although neurotransmitter respecification can potentially explain many nervous system adaptations, it is only one of several candidate plasticity mechanisms activated by physiological or pathophysiological changes. Internal or external stimuli could also initiate other adaptive mechanisms in the nervous system, such as changes in synapse number and strength, neuronal morphology, excitability, neurogenesis, and apoptosis (38–41). While our results do not exclude the occurrence of multifaceted plasticity processes, since the number of spinal motoneurons remained unchanged under the applied perturbations (Fig. 2*B*), our observed changes are not likely due to neurogenesis or potential dedifferentiation of the adult interneurons to motoneurons. Given the time courses of our experimental procedures, we thus conclude that motoneuron transmitter respecification does not involve programmed cell death and replacement of spinal motoneurons. Accordingly, other studies have shown that activity-dependent neurotransmitter respecification in vertebrates involves neither neurogenesis nor apoptosis (17, 35). Hence, our results reinforce the notion that the presence of a reserve pool of fast motoneurons enables a motor function-enhancing mechanism in vertebrates.

We still need to determine how a subset of spinal motoneurons acquire the glutamatergic phenotype, the signaling pathways that initiate motoneuron neurotransmitter switching, and the potential involvement of signals from muscle activity in neurotransmitter changes. However, 80 y after the discovery of the cholinergic nature of the vertebrate NMJ (9) we now have a better understanding regarding the capacity and the dynamics of the adult motoneurons to cotransmit glutamate alongside ACh to control motor behaviors.

Materials and Methods

Experimental Animals. All animals were raised and kept in a core facility at the Karolinska Institute according to established procedures. Adult zebrafish (*Danio rerio*; 9–10 wk old; length: 16–19 mm; weight: 0.03–0.05 g) wild type (AB/Tübingen) were used in this study. All experimental protocols were approved by the local Animal Research Ethical Committee, (Stockholm; ethical permit no. 9248-2017) and were performed in accordance with European Union guidelines for the care and use of laboratory animals (86/609/CEE). All efforts were made to utilize only the minimum number of experimental animals necessary to obtain reliable scientific data.

Motoneuron Labeling. Retrograde labeling of axial motor neurons was performed in anesthetized zebrafish with 0.03% tricaine methane sulfonate (MS-222, E10521; Sigma-Aldrich) by using dye injections with tetramethylrhodamine-dextran (3,000 molecular weight, D3307; Thermo Fisher) or with biotinylated dextran (3,000 molecular weight, D7135; Thermo Fisher) into all muscles or into

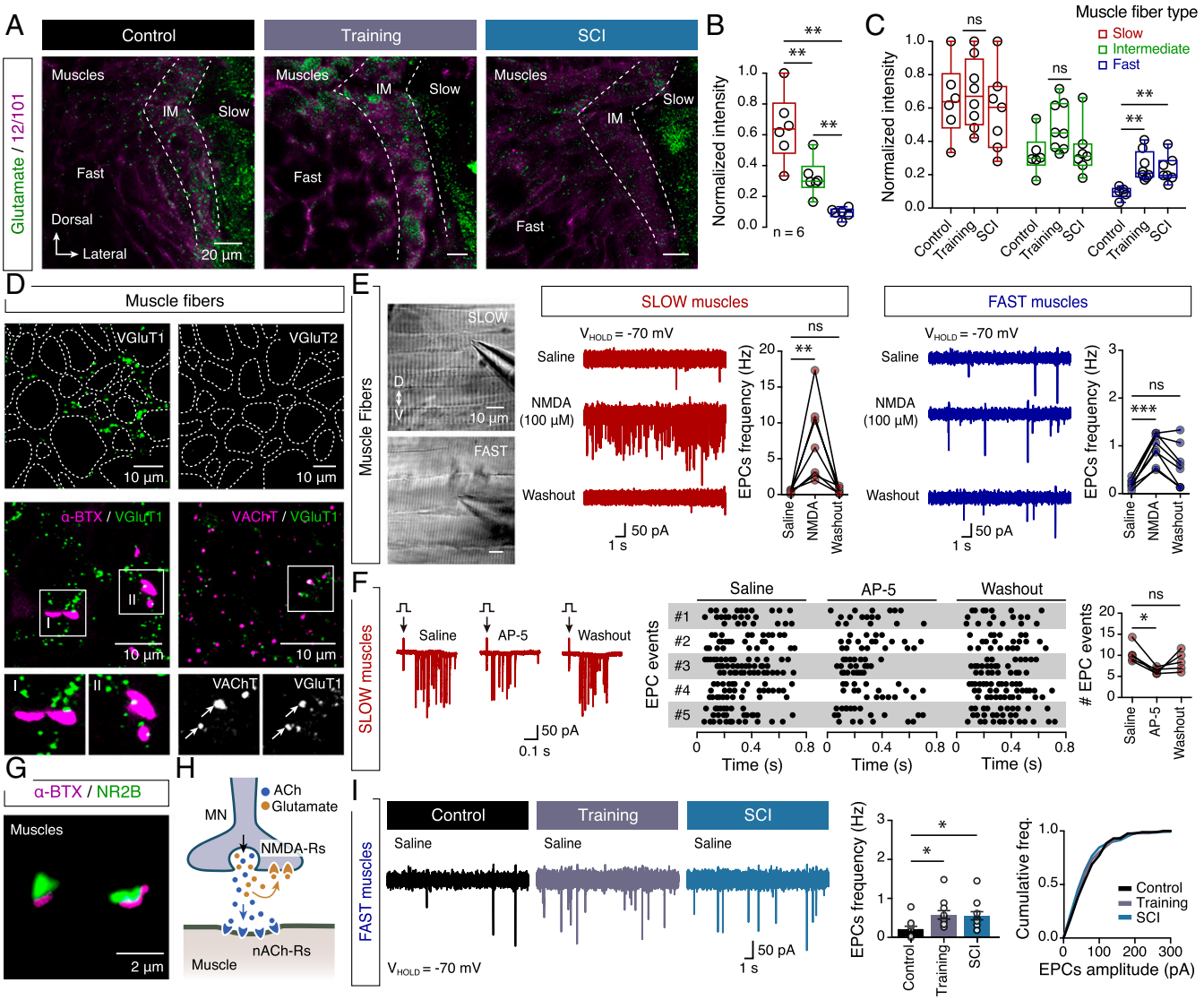

Fig. 5. Neuromuscular effects of glutamate. (*A*) Distribution of glutamate in indicated types of muscle fibers in control animals and after training and after SCI. (*B* and *C*) Quantification of the normalized intensity of the glutamate staining in different muscle fibers ($P = 0.0006$, RM one-way ANOVA) and after the training and SCI (fast: $P = 0.0022$, one-way ANOVA). (*D*) Expression of VGluT1, but not VGluT2, in the area surrounding the muscle fibers (dotted borders); VGluT1 expression near NMJs (indicated by α-BTX) and in close proximity to or colocalized with the expression of the vesicular ACh transporter (VAChT, Arrow). (*E*) Microphotograph of isolated axial muscles from adult zebrafish used for whole-cell voltage-clamp recordings. Bath application of NMDA increases the EPC frequency in both slow ($P = 0.0008$, one-way ANOVA, $n = 7$ zebrafish) and fast muscle fibers ($P = 0.0006$, one-way ANOVA, $n = 8$ zebrafish). (*F*) EPCs events ($n = 5$ zebrafish/3 sweeps) induced after stimulation (arrows; onset, 0 s) were significantly decreased in presence of the selective NMDA receptor antagonist AP-5 (50 µM; $P = 0.0279$, RM one-way ANOVA). (*G*) Expression of NMDA receptor subunit 2B (green) in motoneuron terminals at NMJs (indicated by α-BTX; magenta). (*H*) Proposed model of adult zebrafish NMJs. (*I*) Fast muscle fibers showed a significant increase in EPC frequencies following training and SCI ($P = 0.0191$, one-way ANOVA). Whole-cell voltage-clamp recordings were obtained at a holding potential of −70 mV in all recordings. Data are presented as mean ± SEM and as box plots showing the median and 25th and 75th percentile (box and line) and minimal and maximal values (whiskers). $^*P < 0.05$; $^{**}P < 0.01$; $^{***}P < 0.001$; ns, not significant. For detailed statistics see *SI Appendix*, Table S1.

specific muscle fiber types (slow, intermediate, or fast) in myotomes 14–16 (21, 42, 43). All of the injected animals were allowed to recover for 5 h to overnight to help the retrograde transport of the tracer.

Immunohistochemistry. All animals were deeply anesthetized with 0.1% MS-222. The spinal cords were then extracted and fixed in 4% paraformaldehyde (PFA) and 5% saturated picric acid (P6744; Sigma-Aldrich) in PBS (0.01 M; pH = 7.4) at 4 °C for 2–14 h. We performed whole-mount immunolabeling in spinal cords as follows. The tissue was washed three times for 5 min in PBS. Nonspecific protein binding sites were blocked with 4% normal donkey serum (NDS, D9663; Sigma-Aldrich) with 1% BSA (A2153; Sigma-Aldrich) and 1% Triton X-100 (T8787; Sigma-Aldrich) in PBS for 1 h at room temperature (RT). Primary antibodies (*SI Appendix*, Table S2) were diluted in 1% of blocking solution and applied for 1–3 d at 4 °C. After thorough buffer rinses the tissues were then incubated with the appropriate secondary antibodies (*SI Appendix*, Table S2) diluted 1:500 and with streptavidin conjugated to Alexa Fluor 488 (1:500, S32354; Thermo Fisher) Alexa Fluor 555 (1:500, S32355; Thermo Fisher) or Alexa Fluor 647 (1:500, S32357; Thermo Fisher) in 1% Triton X-100 (T8787; Sigma-Aldrich) in PBS overnight at 4 °C. Finally, the tissue was thoroughly rinsed in PBS and cover-slipped with fluorescent hard medium (H-1400; VectorLabs).

For muscle fiber immunohistochemistry and morphometric analysis, experimental animals were anesthetized with 0.1% MS-222. The skin was carefully removed and the animal fully decapitated at the precaudal level corresponding to myotome 6 and fixed in 4% PFA in phosphate buffer saline (0.01 M; pH = 7.4) at 4 °C for 14 h. The tissue was then cryoprotected by overnight incubation in 30% (wt/vol) sucrose in PBS at 4 °C, embedded in optimal cutting temperature cryomount (45830; Histolab) and rapidly frozen

in dry-ice-cooled isopentane (2-methylbutane, 277258; Sigma-Aldrich) at approximately −35 °C. Transverse coronal plane cryosections (thickness: 25 μm) of the whole myotome (myotome 15) were collected on gelatin-covered slides and processed for immunohistochemistry. The sections were washed three times for 5 min in PBS. Nonspecific protein binding sites were blocked with 2.5% NDS (D9663; Sigma-Aldrich) with 3% BSA (A2153; Sigma-Aldrich) and 1% Triton X-100 (T8787; Sigma-Aldrich) in PBS for 1 h at RT. Primary and secondary antibodies were applied as described above for the spinal cord tissue.

For localization of NMJs, Alexa Fluor 488-conjugated α-BTX (1:500, B13422; Thermo Fisher) was applied together with the primary antibodies.

Swim Training Paradigm and Critical Speed Test. Animals of the same size [body length (BL) and body depth] and weight were used in the swim training paradigm. Initially, some of the designated animals (n = 10 zebrafish) were randomly selected and subjected to the critical speed (U_{CRIT}) test using a commercially available swim tunnel (5 L, SW10050; Loligo Systems). U_{CRIT} is a measure of the highest sustainable swimming speed that a fish can reach (44). The zebrafish were subjected to time intervals of flow velocity (increments of 4.5 cm/s in 5-min steps) until the fish were unable to swim against the water current (fatigued; *SI Appendix*, Fig. S1). Fatigue was determined when fish stopped swimming and were forced against the rear net of the tunnel for more than 5 s. Critical speed was calculated in all cases using the following equation (*SI Appendix*, Fig. S1 and ref. 44):

$$U_{CRIT} = U_{FATIGUE} + [U_{STEP} \times (t_{FATIGUE}/t_{STEP})],$$

where $U_{FATIGUE}$ is the highest flow velocity at which fish swam for the whole interval, U_{STEP} is the velocity increment, $T_{FATIGUE}$ is the time that fish swam in the last interval at final velocity, and T_{STEP} is the duration of one interval.

For the swim training, a grouped long-term exercise training protocol was applied, in which exercised/trained zebrafish (~20) swam at 60% of U_{CRIT} for 6 h per day, 5 d per week, for four consecutive weeks. After the exercise period, fish were randomly assigned to a short-term experimental group or long-term (recovery) group. Animals of the recovery group were maintained in standard conditions for 4 wk. In all cases after the experimental period the animals were anesthetized, their motoneurons were labeled with retrograde tracers (as described in *Motoneuron Labeling*), and they were processed for immunohistochemistry (as described in *Immunohistochemistry*). The critical speed was normalized to BL of the experimental animals and is expressed as BL per s.

Open Field Test. For the open field test, animals were placed in small dishes (diameter: 8 cm) and allowed to swim freely, while their swimming was recorded for 5 min (15 min after they were placed in the arena). Their swimming behavior recorded during a 3-min period was analyzed after optimization and implementation of wrMTrck, a freely available ImageJ plugin. The experimental animals' average velocity and maximum velocity were normalized to their BL and are expressed as BL per s.

SCI. Zebrafish were anesthetized in 0.03% tricaine methane sulfonate (MS-222; Sigma-Aldrich) before subjection to the SCI treatment, which involved complete transection at the level of spinal cord segment 10, with a microknife (10318-14; Fine Science Tools) under constant visual control. Once the lesion was completed, the spinally transected animals were kept in fresh water under standard conditions for 48 h (short-term experiments) or 4 wk (long-term recovery experiments).

Sterile Inflammation. Animals were anesthetized in 0.03% tricaine methane sulfonate (MS-222; Sigma-Aldrich) in fish water and injected intraperitoneally (volume: 2 μL) with saline, LPS (10 mg/mL, L2630; Sigma-Aldrich), or zymosan (10 mg/mL, Z4250; Sigma-Aldrich) in saline, as previously described (22). Treated animals were then placed in aquaria and allowed to survive for 6 d before the retrograde labeling of motoneurons (as described in *Motoneuron Labeling*) and allowed to survive for an additional 24 h. During the sterile inflammation treatment all animals were kept under the standard housing conditions.

Electrophysiology. Adult zebrafish were cold-anesthetized in a slush of frozen extracellular solution containing MS-222. The skin was removed to allow access to the axial muscles. The myotomes were dissected out carefully without the spinal cord and transferred to a recording chamber that was continuously perfused with an extracellular solution containing 135.2 mM NaCl, 2.9 mM KCl, 2.1 mM $CaCl_2$, 10 mM Hepes, and 10 mM glucose, pH 7.8, adjusted with NaOH, and an osmolarity of 290 mOsm. For whole-cell intracellular recordings from muscle fibers in voltage-clamp mode, electrodes (resistance, 3–5 MΩ) were pulled from borosilicate glass (outer diameter, 1.5 mm; inner diameter, 0.87 mm; Hilgenberg) on a micropipette puller (model P-97; Sutter Instruments) and filled with intracellular solution containing the following: 120 mM K-gluconate, 5 mM KCl, 10 mM Hepes, 4 mM Mg_2ATP, 0.3 mM Na_4GTP, 10 mM Na-phosphocreatine, pH 7.4, adjusted with KOH, and osmolarity of 275 mOsm. Muscle fibers were visualized using a microscope (LNscope; Luigs & Neumann) equipped with a CCD camera (Lumenera) and were then targeted specifically. Intracellular patch-clamp electrodes were advanced to the myotomes using a motorized micromanipulator (Luigs & Neumann) while applying constant positive pressure. Intracellular signals were amplified with a MultiClamp 700B intracellular amplifier (Molecular Devices). Fibers were clamped at −70 mV throughout all EPC recordings. All experiments were performed at RT (23 °C).

The following drugs (prepared by diluting stock solutions in distilled water) were added (singly or in combinations mentioned in the text) to the physiological solution: NMDA (100 μM, M3262; Sigma-Aldrich), the selective NMDA-receptor antagonist AP-5 (50 μM, A5282; Sigma-Aldrich), and the nicotinic ACh receptor antagonists (+)-tubocurarine hydrochloride (*d*-tubocurarine, 10 μM, T2379; Sigma-Aldrich) and α-BTX (10 μM, T0195; Sigma-Aldrich). EPC frequencies were recorded for 15- to 20-s periods under all conditions: 10 s before application of the NMDA agonist, 10 s after the NMDA bath application, and 30 s after the NMDA washout. For the experiments with the selective choline uptake blocker hemicholinium-3, isolated muscles were preincubated with hemicholinium-3 (50 μM, H108; Sigma-Aldrich) and NMDA (100 μM) for 15 min. To block postsynaptic NMDA receptors selectively, the intracellular solution was supplemented with the noncompetitive antagonist MK-801 (1 mM, M107; Sigma-Aldrich).

To examine the direct effect of motoneuron action potential-driven release in NMJs we performed split-bath experiments. For this, the perfusion was separated between the rostral part of the preparations and the caudal axial muscles at segments 15–20 (*SI Appendix*, Fig. S6). This configuration allowed selective blockage of the muscle NMDA receptors, by 50 μM AP-5, while the rostral spinal cord was constantly perfused with physiological solution. A single electrical stimulation was delivered in each spinal cord at segments 2–4, while patch-clamp recordings of EPCs were acquired from slow muscle fibers at segments 20–24 (*SI Appendix*, Fig. S6). For every recorded muscle fiber three sweeps of electrical stimulation were delivered under each condition (control, after AP-5 application, and washout) at 1-min time intervals. The EPC events were detected in semiautomatic (supervised) fashion after baseline subtraction using AxoGraph (version X 1.5.4; RRID: SCR_014284; AxoGraph Scientific) or Clampfit (version 10.6; Molecular Devices) software.

Analysis. Images of the adult zebrafish spinal cord preparations were acquired using an LSM 800 laser scanning confocal microscope (Zeiss) with a 40× objective. For each examined whole-mount preparation, the whole hemisegment of the spinal cord (from lateral side to medial area of the central canal) was scanned, generating a z-stack (z-step size = 0.5–1 μm). Cells were counted in segment 15. Relative positions of the somata of the neurons within the spinal cord were estimated (using the lateral, dorsal, and ventral edges of the cord and central canal as landmarks) and soma sizes were measured using ImageJ (NIH; ref. 45). To enhance visualization of our data, most of the whole-mount images presented here were obtained by merging subsets of the original z-stacks. For analysis of the zebrafish musculature, perimeters of individual muscle fibers were manually traced in the confocal microphotographs of each muscle sample using ImageJ. Images of fast muscle fibers presented in the figures were obtained from the epaxial area at even distances from the horizontal septum, midline, and edge of the myotome. Images of the slow and intermediate muscle fibers were acquired near the horizontal septum and close to the skin. For the $mef2^+$ cells, profiles of the labeled cells were counted manually in the whole section (myotome 15). Analysis of the glutamate intensity in the different muscle fiber types was performed using ImageJ, followed from data normalization to the highest intensity levels between each group of tested conditions. High-resolution confocal images of NMJs labeled with α-BTX and NR2B (Fig. 5*G*) were further processed by 3D deconvolution using DeconvolutionLab2 software (EPFL; ref. 46) to allow assessment of the overlap between the different receptors located in pre- or postsynaptic membranes.

All figures and graphs were prepared with Adobe Photoshop and Adobe Illustrator (Adobe Systems Inc.). Digital modifications of the images (brightness and contrast) were minimal to minimize potential distortion of biological information. All double-labeled immunofluoresence images were converted to magenta-green to improve visualization of the results for colorblind readers.

Statistics. The significance of differences between the means in experimental groups and conditions was analyzed using either parametric tests (for larger data samples), two-tailed unpaired Student's *t* test, or one-way ANOVA (ordinary or repeated measures) followed by post hoc Tukey's test or Dunnett's multiple comparison test, or nonparametric tests (for small data samples) Wilcoxon test, using Prism (GraphPad Software Inc.). Significance levels indicated in all figures are as follows: $*P < 0.05$, $**P < 0.01$, $***P < 0.001$, $****P < 0.0001$. All data are presented as mean ± SEM or as box plots showing the median and 25th and 75th percentile (box and line) and minimal and maximal values (whiskers). Finally, the *n* values indicate the final number of validated animals per group or the number of cells that were evaluated.

ACKNOWLEDGMENTS. We thank Drs. Sten Grillner, Mario Wullimann, Mark Masino, Marie Carlén, Konstantinos Meletis, Paul Williams, and members of the K.A. laboratory for their valuable discussion, comments, contributions to the project, and assistance in preparing this paper. This work was supported by Swedish Research Council Grant 2015-03359 (to K.A.), StratNeuro (K.A.), Swedish Brain Foundation Grant FO2016-0007 (to K.A.), Erik and Edith Fernström Foundation Grant FS-2017:0005 (to K.A.), and Längmanska kulturfonden Grant BA17-0390 (to K.A.).

1. Rogawski MA, Barker JL (1986) *Neurotransmitter Actions in the Vertebrate Nervous System* (Springer, New York), p 511.
2. Schwartz JH (2000) Neurotransmitters. *Principles of Neural Science*, eds Kandel ER, Schwartz JH, Jessell TM (Elsevier, New York), pp 280–295.
3. Jessell TM (2000) Neuronal specification in the spinal cord: Inductive signals and transcriptional codes. *Nat Rev Genet* 1:20–29.
4. Lee SK, Pfaff SL (2001) Transcriptional networks regulating neuronal identity in the developing spinal cord. *Nat Neurosci* 4(Suppl):1183–1191.
5. Goulding M (2009) Circuits controlling vertebrate locomotion: Moving in a new direction. *Nat Rev Neurosci* 10:507–518.
6. Arber S (2012) Motor circuits in action: Specification, connectivity, and function. *Neuron* 74:975–989.
7. Lu DC, Niu T, Alaynick WA (2015) Molecular and cellular development of spinal cord locomotor circuitry. *Front Mol Neurosci* 8:25.
8. Kiehn O (2016) Decoding the organization of spinal circuits that control locomotion. *Nat Rev Neurosci* 17:224–238.
9. Dale HH, Feldberg W, Vogt M (1936) Release of acetylcholine at voluntary motor nerve endings. *J Physiol* 86:353–380.
10. Eccles JC, Fatt P, Koketsu K (1954) Cholinergic and inhibitory synapses in a pathway from motor-axon collaterals to motoneurones. *J Physiol* 126:524–562.
11. Curtis DR, Ryall RW (1964) Nicotinic and muscarinic receptors of Renshaw cells. *Nature* 203:652–653.
12. Meister B, et al. (1993) Glutamate transporter mRNA and glutamate-like immunoreactivity in spinal motoneurones. *Neuroreport* 5:337–340.
13. Herzog E, et al. (2004) Expression of vesicular glutamate transporters, VGLUT1 and VGLUT2, in cholinergic spinal motoneurons. *Eur J Neurosci* 20:1752–1760.
14. Mentis GZ, et al. (2005) Noncholinergic excitatory actions of motoneurons in the neonatal mammalian spinal cord. *Proc Natl Acad Sci USA* 102:7344–7349.
15. Nishimaru H, Restrepo CE, Ryge J, Yanagawa Y, Kiehn O (2005) Mammalian motor neurons corelease glutamate and acetylcholine at central synapses. *Proc Natl Acad Sci USA* 102:5245–5249.
16. Black IB, et al. (1984) Neurotransmitter plasticity at the molecular level. *Science* 225: 1266–1270.
17. Dulcis D, Jamshidi P, Leutgeb S, Spitzer NC (2013) Neurotransmitter switching in the adult brain regulates behavior. *Science* 340:449–453.
18. Vaaga CE, Borisovska M, Westbrook GL (2014) Dual-transmitter neurons: Functional implications of co-release and co-transmission. *Curr Opin Neurobiol* 29:25–32.
19. Spitzer NC (2017) Neurotransmitter switching in the developing and adult brain. *Annu Rev Neurosci* 40:1–19.
20. Spitzer NC (2012) Activity-dependent neurotransmitter respecification. *Nat Rev Neurosci* 13:94–106.
21. Ampatzis K, Song J, Ausborn J, El Manira A (2013) Pattern of innervation and recruitment of different classes of motoneurons in adult zebrafish. *J Neurosci* 33: 10875–10886.
22. de Preux Charles A-S, Bise T, Baier F, Sallin P, Jaźwińska A (2016) Preconditioning boosts regenerative programmes in the adult zebrafish heart. *Open Biol* 6:160101.
23. Palstra AP, et al. (2010) Establishing zebrafish as a novel exercise model: Swimming economy, swimming-enhanced growth and muscle growth marker gene expression. *PLoS One* 5:e14483.
24. Song J, Ampatzis K, Björnfors ER, El Manira A (2016) Motor neurons control locomotor circuit function retrogradely via gap junctions. *Nature* 529:399–402.
25. Shigeri Y, Seal RP, Shimamoto K (2004) Molecular pharmacology of glutamate transporters, EAATs and VGLUTs. *Brain Res Brain Res Rev* 45:250–265.
26. Weihe E, Tao-Cheng JH, Schäfer MK, Erickson JD, Eiden LE (1996) Visualization of the vesicular acetylcholine transporter in cholinergic nerve terminals and its targeting to a specific population of small synaptic vesicles. *Proc Natl Acad Sci USA* 93:3547–3552.
27. Fu WM, Liu JJ (1997) Regulation of acetylcholine release by presynaptic nicotinic receptors at developing neuromuscular synapses. *Mol Pharmacol* 51:390–398.
28. Fu WM, Liou HC, Chen YH, Wang SM (1998) Coexistence of glutamate and acetylcholine in the developing motoneurons. *Chin J Physiol* 41:127–132.
29. Todd KJ, Slatter CAB, Ali DW (2004) Activation of ionotropic glutamate receptors on peripheral axons of primary motoneurons mediates transmitter release at the zebrafish NMJ. *J Neurophysiol* 91:828–840.
30. Waerhaug O, Ottersen OP (1993) Demonstration of glutamate-like immunoreactivity at rat neuromuscular junctions by quantitative electron microscopic immunocytochemistry. *Anat Embryol (Berl)* 188:501–513.
31. Berger UV, Carter RE, Coyle JT (1995) The immunocytochemical localization of N-acetylaspartyl glutamate, its hydrolysing enzyme NAALADase, and the NMDAR-1 receptor at a vertebrate neuromuscular junction. *Neuroscience* 64:847–850.
32. Barthélémy-Requin M, Bévengut M, Portalier P, Ternaux JP (2006) Release of glutamate by the embryonic spinal motoneurons of rat positively regulated by acetylcholine through the nicotinic and muscarinic receptors. *Neurochem Int* 49:584–592.
33. Borodinsky LN, Spitzer NC (2007) Activity-dependent neurotransmitter-receptor matching at the neuromuscular junction. *Proc Natl Acad Sci USA* 104:335–340.
34. Kraus T, Neuhuber WL, Raab M (2004) Vesicular glutamate transporter 1 immunoreactivity in motor endplates of striated esophageal but not skeletal muscles in the mouse. *Neurosci Lett* 360:53–56.
35. Borodinsky LN, et al. (2004) Activity-dependent homeostatic specification of transmitter expression in embryonic neurons. *Nature* 429:523–530.
36. Dulcis D, Spitzer NC (2012) Reserve pool neuron transmitter respecification: Novel neuroplasticity. *Dev Neurobiol* 72:465–474.
37. Spitzer NC (2015) Neurotransmitter switching? No surprise. *Neuron* 86:1131–1144.
38. Abbott LF, Nelson SB (2000) Synaptic plasticity: Taming the beast. *Nat Neurosci* 3: 1178–1183.
39. Cohen EJ, Quarta E, Bravi R, Granato A, Minciacchi D (2017) Neural plasticity and network remodeling: From concepts to pathology. *Neuroscience* 344:326–345.
40. Schulz DJ, Lane BJ (2017) Homeostatic plasticity of excitability in crustacean central pattern generator networks. *Curr Opin Neurobiol* 43:7–14.
41. Sweatt JD (2016) Neural plasticity and behavior–Sixty years of conceptual advances. *J Neurochem* 139(Suppl 2):179–199.
42. Berg EM, Bertuzzi M, Ampatzis K (2018) Complementary expression of calcium binding proteins delineates the functional organization of the locomotor network. *Brain Struct Funct* 223:2181–2196.
43. Bertuzzi M, Ampatzis K (2018) Spinal cholinergic interneurons differentially control motoneuron excitability and alter the locomotor network operational range. *Sci Rep* 8:1988.
44. Brett JR (1964) The respiratory metabolism and swimming performance of young sockeye salmon. *J Fish Res Board Can* 21:1183–1226.
45. Schneider CA, Rasband WS, Eliceiri KW (2012) NIH image to ImageJ: 25 years of image analysis. *Nat Methods* 9:671–675.
46. Sage D, et al. (2017) DeconvolutionLab2: An open-source software for deconvolution microscopy. *Methods* 115:28–41.